Anisotropic contributions to the ^{119}Sn transferred hyperfine fields in $R\mathrm{Mn}_6\mathrm{Sn}_{6-x}X_x$ (R=Y,Tb,Er; X=In,Ga)

Laura K. Perry,[1] D. H. Ryan,[2] and G. Venturini[3]
[1]*Centre for the Physics of Materials and Physics Department, McGill University, Montréal, Quebec H3A 2T8, Canada*
[2]*Centre for the Physics of Materials and Physics Department, McGill University, 3600 University Street, Montréal, Quebec H3A 2T8, Canada*
[3]*Laboratoire de Chimie du Solide Minéral, Université Henri Poincaré-Nancy I, Associé au CNRS (UMR 7555), BP 239, 54506 Vandoeuvre les Nancy Cedex, France*
(Received 14 November 2006; published 17 April 2007)

The anisotropic contribution to the transferred hyperfine fields in $\mathrm{YMn}_6\mathrm{Sn}_{5.42}\mathrm{In}_{0.58}$ has been isolated using a field-driven moment rotation from the *ab* plane to the *c* axis in a single crystal. We find that at 12 K, the anisotropic contribution is between 3% and 4% of the total field for the Sn 2*c* and Sn 2*d* sites, while it accounts for nearly one-third of the observed field at the Sn 2*e* site. Comparison with data from $R\mathrm{Mn}_6\mathrm{Sn}_{6-x}X_x$ (R=Tb,Er; X=Ga,In) compounds containing magnetic rare earths shows that the Mn and R contributions to the anisotropic component of the transferred hyperfine fields are similar in magnitude.

DOI: 10.1103/PhysRevB.75.144417 PACS number(s): 76.80.+y, 75.50.Ee

I. INTRODUCTION

At a Sn site in a crystal structure, any hyperfine field B_{hf} must be transferred to it from neighboring magnetic moments. This transferred hyperfine field is the sum of isotropic and anisotropic contributions, although it is often assumed to be totally isotropic. There are three main contributions to the total transferred hyperfine field: orbital, Fermi contact (isotropic), and dipolar (anisotropic) fields. Because of spin-orbit coupling, the spin polarization of the Sn *p* states induces an orbital polarization, creating an orbital field. It is generally assumed to be small and omitted from calculations of the total transferred hyperfine field.[1] Polarization of conduction electrons induces a spin imbalance at the Sn nucleus. This generates the Fermi contact field, which depends only on the magnitude of the neighboring moments and the symmetry of their magnetic structure. Finally, the nonspherical valence *p* spin density of Sn (which results from the hybridization with the spin-polarized *d* states of neighboring transition-metal atoms) leads to the dipolar field, which depends not only on the magnitude of the neighboring moments but also on the relative orientations of those moments and their connecting bonds. The total hyperfine field transferred to a Sn site, first expressed in the case of MnSn_2,[2] is given by

$$\mathbf{B}_{hf} = \left[A_p \sum_{i=1}^{6} \mathbf{u}_i (\vec{\mu}_i \cdot \mathbf{u}_i) - \frac{A_p}{3} \sum_{i=1}^{6} \vec{\mu}_i \right] + A_s \sum_{i=1}^{6} \vec{\mu}_i, \qquad (1)$$

where $\mathbf{u}_i$ is the unit vector connecting each Sn atom to a specific Mn atom with moment $\vec{\mu}_i$, and A_p and A_s are the dipolar and contact fields due to a unit Mn moment. A_p is also referred to as the anisotropic constant. The last term in Eq. (1) is the isotropic contribution from the Mn shells around the Sn atoms, while the first two terms (in brackets) represent the anisotropic part of the transferred hyperfine field.

For Sn atoms, the anisotropic field A_p can amount to several Teslas.[2–4] For example, there are four Sn sites in the tetragonal CuAl_2-type MnSn_2. The largest observed field is 21.2(2) T and includes both isotropic and anisotropic contributions.[2] However, at one site, the isotropic contribution cancels, leaving a purely anisotropic field of 4.9(2) T (Ref. 2)—almost a quarter of the largest field observed. While it is clear that the anisotropic term constitutes a significant fraction of the total observed field and should, therefore, be included in any analysis of transferred hyperfine fields, as we will show below, the magnitude of the anisotropic contribution is highly variable, even from site to site within the same material.

There are three Sn sites in compounds of the $\mathrm{HfFe}_6\mathrm{Ge}_6$-type $R\mathrm{Mn}_6\mathrm{Sn}_{6-x}X_x$ (R=rare earth; X=Ga,In) family, thus providing three environments in which to study the anisotropic field. However, the anisotropic contribution cannot be identified directly as in MnSn_2 (Ref. 2) or FeSn_2 (Ref. 3) because the crystal and magnetic symmetries are such that there is no cancellation of the isotropic field for any of the three Sn sites. By rotating the magnetic structure relative to the crystal structure, the anisotropic contribution can be isolated because it is the only one of the two contributions which depends on the bonding of Sn with its magnetic neighbors. $R\mathrm{Mn}_6\mathrm{Sn}_6$ compounds with R=Tb, Dy, and Ho undergo a spontaneous temperature-driven spin reorientation, whereby the moments rotate by as much as 90°.[5] The reorientation is caused by the interplay between the anisotropies of the two sublattices, R and Mn. Through the magnitude of the change in B_{hf} due to the reorientation, we can determine the total anisotropic contribution A_p.

The magnitude of A_p can equally be obtained by applying an external field perpendicular to the moment direction and forcing the moments to rotate. In a recent study,[6] we determined the anisotropic contribution by inducing a spin flop in $\mathrm{TbMn}_6\mathrm{Sn}_{5.46}\mathrm{In}_{0.54}$ single crystals. While both methods (temperature and field induced) allow the total anisotropic contribution to be determined, we are unable to distinguish how much each magnetic sublattice contributes to A_p. We can isolate the Mn sublattice's contribution by using a nonmagnetic R such as Hf, Sc, Y, or Lu. Since the magnetocrystalline anisotropy of Mn is relatively weak, in ferromagnetic

$YMn_6Sn_{6-x}In_x$ single crystals [ordered in the *ab* plane below $T_C \sim 320$ K for $x > 0.4$ (Ref. 7)], we can force the Mn moments to rotate onto the *c* axis by applying a large enough external field along *c*.

Here, we use ^{119}Sn Mössbauer spectroscopy to examine the anisotropic Sn hyperfine field arising from the Mn sublattice in $YMn_6Sn_{5.42}In_{0.58}$ and draw comparisons with its magnitude in other systems, such as $TbMn_6Sn_{6-x}X_x$ [X=In (Ref. 6), Ga (Ref. 8)] and $ErMn_6Sn_{5.89}Ga_{0.11}$.[9] A significant anisotropic contribution from the *R* sublattice is inferred, indicating that the model embodied by Eq. (1) is too simple.

II. EXPERIMENTAL METHODS

The flux method used to obtain the $YMn_6Sn_{5.42}In_{0.58}$ single crystal has been described elsewhere.[10] For the current study, the overall starting composition was $YMn_6Sn_{26}In_{54}$ and the crystals were grown in a 973–673 K temperature range. The $HfFe_6Ge_6$ crystal structure was checked on ground crystals by powder x-ray diffraction (Guinier camera, Co $K\alpha$) and the fitted cell parameters were a=5.536(1) Å and c=9.053(2) Å. The indium content in the crystals was verified using microprobe analysis and found to be x=0.58(5). A neutron-diffraction study of the related compound $TmMn_6Sn_5In$ revealed that the In atoms were mainly located on the Sn 2*d* site of the $HfFe_6Ge_6$ structure,[11] while x-ray single-crystal refinement for $TmMn_6Sn_{5.2}In_{0.8}$ led to the following atomic coordinates: z_{Mn}=0.2462(1) and $z_{Sn\,2e}$ =0.3359(1).[12]

The $YMn_6Sn_{5.42}In_{0.58}$ sample used for the Mössbauer work was constructed as a mosaic of single crystal platelets which had their *c* axis perpendicular to the plane of the plates. ^{119}Sn transmission Mössbauer spectra were collected using a 10 mCi ^{119m}Sn $CaSnO_3$ source mounted on a spectrometer operating in sine mode and calibrated using α-Fe and a ^{57}Co source. A 25 μm Pd filter was used to absorb the Sn Kα x rays also emitted by the source. Both the sample and the source were held at 12 K in a helium-flow cryostat, and magnetic fields from 0 to 6 T were applied parallel to the γ beam and, hence, also parallel to the crystal *c* axis. The superconducting split solenoid magnet has a bucking coil that provides a field-free region at the location of the source to avoid field-broadening effects. All of the spectra were fitted with a conventional nonlinear least-squares minimization routine, which uses a sum of Lorentzian line shapes whose line positions are calculated as a first-order perturbation. Basic magnetic characterization was carried out on a commercial 9 T magnetometer, manufactured by Quantum Design.

The local electric-field gradient (efg) provides a crystallographic reference frame within which a change in moment direction can be observed using Mössbauer spectroscopy. The efg tensor can be diagonalized, and the largest component in the diagonal form (V_{zz}) is conventionally taken as defining the *z* axis for the efg coordinate system. The high point symmetries of the three Sn sites in RMn_6Sn_6 (6*mm* for Sn 2*e* and $\bar{6}m2$ for Sn 2*c* and Sn 2*d*) cause the crystallographic and efg axes to coincide, guaranteeing that the *z* axis of the efg tensor lies along *a*, *b*, or *c*. The local hexagonal point symmetries also impose axial symmetry (i.e., $V_{xx} = V_{yy} \Rightarrow \eta = 0$), such that the observed quadrupole shift Δ is

$$\Delta = \frac{eQV_{zz}}{4}(3\cos^2\theta - 1), \tag{2}$$

where θ is the angle between the *z* axis of the efg and B_{hf} at the Sn site due to the surrounding magnetic moments. For $\theta = 90°$, $\Delta = -\frac{1}{4}eQV_{zz}$ and for $\theta = 0°$, $\Delta = \frac{1}{2}eQV_{zz}$, so that a change in Δ by a factor of −2 corresponds to a change in moment direction by 90°.

For a single crystal or highly textured sample, an additional Mössbauer parameter can be used: the intensity of the second and fifth Mössbauer lines relative to the third and fourth lines (R). Writing this intensity ratio as $3:R:1:1:R:3$ for a six-line ^{119}Sn Mössbauer pattern, R is given by

$$R = \frac{4\sin^2\vartheta}{1+\cos^2\vartheta}, \tag{3}$$

where ϑ is the angle between B_{hf} and the axis defined by the γ beam used to make the Mössbauer measurement. For a single crystal, the moments all point along a well-defined direction with respect to the γ axis. For example, the $YMn_6Sn_{5.42}In_{0.58}$ single-crystal platelets grew with *c* perpendicular to the plane of the plates, and so parallel to the γ axis used in the Mössbauer measurement. If the moments are in the *ab* plane, then $\gamma \| c \perp \mu$, giving $\vartheta = 90°$ and R=4. If the moments lie along the *c* axis, then $\gamma \| c \| \mu$, giving $\vartheta = 0°$ and R=0. Thus, for an oriented sample, R can be used to determine the moment direction relative to the γ axis, as well as to the crystal structure, through the ϑ term. When R is either 0 or 4, such as the case for a single crystal, we can also determine the direction of principal axis (*z*) of the efg tensor. For a powdered sample, R averages to 2 and this information is lost.

III. RESULTS

A. Magnetic structure

The magnetic structure of $YMn_6Sn_{6-x}In_x$ depends strongly on In content, *x*, because the substitution enhances the ferromagnetic interactions with respect to the antiferromagnetic ones.[7] The ordering behavior of the parent ternary compound (YMn_6Sn_6) is quite complex, with a narrow antiferromagnetic (AF) region from 350 to 328 K followed by helimagnetic ordering.[13,14] Minimal doping with In suppresses the AF phase, and for $x > 0.15$, the initial ordering becomes ferromagnetic, with further helimagnetic ordering observed below T_t for $x < 0.4$. The magnetic phase diagram for $YMn_6Sn_{6-x}In_x$, constructed using data from Refs. 7 and 13 and including our own data for the $YMn_6Sn_{5.42}In_{0.58}$ alloy studied here, is shown in Fig. 1.

Figure 2 shows the magnetization of a single crystal of $YMn_6Sn_{5.42}In_{0.58}$ in applied fields of up to 7 T at 5 K. The field was applied both perpendicular and parallel to the *c* axis of the crystal platelet. The saturation magnetization [50.1(2) J/T/kg] yields a Mn moment of 1.69(1)μ_B, in excellent agreement with that derived in YMn_6Sn_6 and

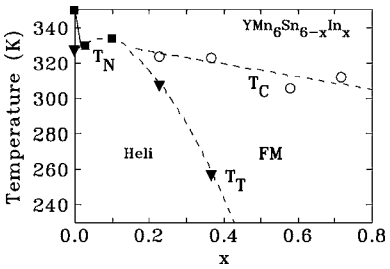

FIG. 1. Magnetic phase diagram for in $YMn_6Sn_{6-x}In_x$ ($0.0 \leqslant x \leqslant 0.72$) showing regions of helimagnetic (Heli) and ferromagnetic (FM) ordering (Refs. 7 and 13). A very narrow region of antiferromagnetic (AF) order is also present at $x=0$.

$ScMn_6Sn_6$ single crystals ($1.67\mu_B$).[13] Both measurements are significantly lower than the $2.57(9)\mu_B$ obtained by neutron scattering from $YMn_6Sn_{5.28}In_{0.72}$.[7] The slow approach to saturation for B_o applied parallel to the c axis confirms that this is an easy-plane system (the Mn moments are ordered in the ab plane) and that ~2.3(2) T is needed to force the moments parallel to the c axis.

B. Mössbauer spectroscopy

The 12 K Mössbauer pattern of $YMn_6Sn_{5.42}In_{0.58}$ in zero applied field is shown in Fig. 3. It was fitted with three sextets corresponding to the three Sn sites of the crystal structure, along with a Sn impurity [isomer shift δ =2.70(2) mm/s relative to $CaSnO_3$ and spectral area 6.7(2)%]. The site assignment closely follows that seen in the $TbMn_6Sn_{6-x}Ga_x$ series[8] as well as that of $MgMn_6Sn_6$.[1] In Table I, we show the Mössbauer parameters of $TbMn_6Sn_{5.8}Ga_{0.2}$ just above T_{sr}=275(5) K where the moments are in the ab plane, and those of $YMn_6Sn_{5.42}In_{0.58}$ and $MgMn_6Sn_6$, for which the Mn moments are in the ab plane across the whole ordered range. These compounds have identical crystal structures and similar magnetic structures. In all cases, the sequence of hyperfine fields is $B_{hf}(\text{Sn } 2c) > B_{hf}(\text{Sn } 2d) > B_{hf}(\text{Sn } 2e)$, and the sequence of quadrupole shifts is $|\Delta(\text{Sn } 2d)| > |\Delta(\text{Sn } 2c)| > |\Delta(\text{Sn } 2e)|$.

Figure 4 (left) shows the Mössbauer spectra of $YMn_6Sn_{5.42}In_{0.58}$ at 12 K as a function of the applied field. The areas were constrained to those determined at 12 K in zero field. The intensity ratio R (Fig. 4, top right) in zero

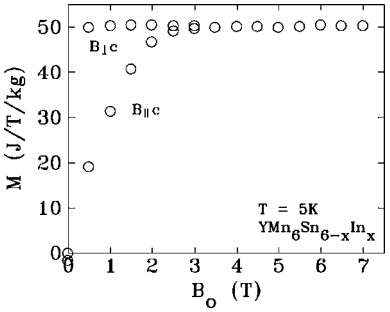

FIG. 2. 5 K magnetization curves for $YMn_6Sn_{5.42}In_{0.58}$ with B_o applied perpendicular and parallel to the c axis.

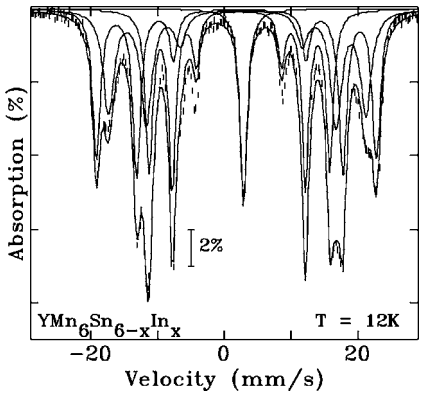

FIG. 3. $YMn_6Sn_{5.42}In_{0.58}$ Mössbauer spectrum at 12 K in zero applied field.

field is 3.39(7), indicating that the moments are in the ab plane. R should be 4 for ab plane ordering and we attribute the reduced value to saturation effects in this rather thick single-crystal sample, which at 150(10) μm is more than twice the thickness of the powder samples that we normally use. However, saturation will not affect the measurement of the field (B_{rot}) required to reduce R to 0. We find B_{rot} =2.1(2) T, consistent with a complete 90° rotation out of the ab plane and in excellent agreement with the field derived from magnetometry. The quadrupole shifts Δ also show the moment rotation, where $\Delta_{B_o>B_{rot}} = -2\Delta_{B_o<B_{rot}}$ within error for all three Sn sites (Fig. 4, bottom right). The factor of −2 change in Δ at B_{rot} indicates that the Mn moments have rotated by a full 90° from the ab plane to the c axis. This result confirms that the low value of R observed in zero field is due to saturation effects and not to the moments being canted out of the ab plane.

In the presence of an externally applied field B_o, the observed hyperfine field B_{hf}^{obs} at a tin site includes two additional contributions,

$$B_{hf}^{obs} = B_{hf}^{trans} - (B_o - B_D), \tag{4}$$

where B_{hf}^{trans} is any transferred hyperfine field including isotropic and anisotropic parts (absent in nonmagnetic environments), and the term in parentheses is due to the applied field, corrected for any demagnetizing field B_D. This second term is negative as the magnetization and resulting hyperfine field are generally antiparallel. The Sn hyperfine fields are shown in Fig. 5 as functions of the applied field. The slope of

TABLE I. Mössbauer parameters of $TbMn_6Sn_{5.8}Ga_{0.2}$ (290 K) (Ref. 8), $YMn_6Sn_{5.42}In_{0.58}$ (12 K), and $MgMn_6Sn_6$ (4.2 K) (Ref. 1).

	$TbMn_6Sn_{5.8}Ga_{0.2}$		$YMn_6Sn_{5.42}In_{0.58}$		$MgMn_6Sn_6$	
$\mu \perp c$ Site	Δ (mm/s)	B_{hf} (T)	Δ (mm/s)	B_{hf} (T)	Δ (mm/s)	B_{hf} (T)
Sn 2c	−0.46(4)	23.56(7)	−0.53(3)	31.50(2)	−0.68(8)	32.5(3)
Sn 2d	−0.72(5)	22.6(1)	−0.69(5)	28.98(4)	−1.00(8)	30.0(3)
Sn 2e	−0.14(3)	13.63(2)	0.03(3)	20.54(3)	0.04(8)	21.7(3)

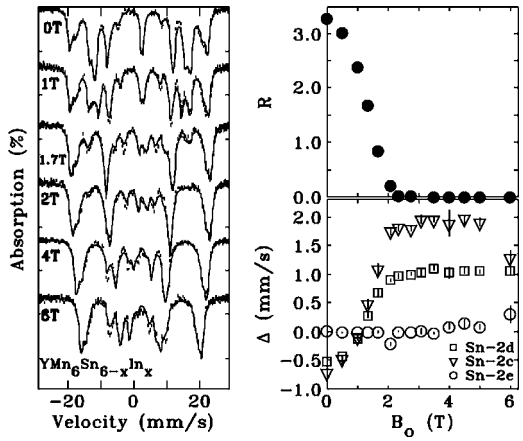

FIG. 4. Left: Mössbauer spectra of $YMn_6Sn_{5.42}In_{0.58}$ at 12 K in applied fields from 0 to 6 T. Top right: intensity ratio R. Bottom right: quadrupole shift of the three Sn sites as functions of applied field. From the B_o dependence of R, we get B_{rot}=2.1(2) T, above which the Mn moments are parallel to the c axis.

the applied field dependence of B_{hf} for the (nonmagnetic) Sn impurity provides a cross-check of both the applied field and the spectrometer calibration. This slope is measured to be +0.97(3), consistent with +1 as expected. While the moments are in the ab plane, the hyperfine fields at all three of the Sn sites show little dependence on B_o because, until the system saturates, the internal field remains essentially zero due to the large demagnetization factor associated with this geometry ($B_o \sim B_D$). When the moments rotate onto the c axis for $B_o > B_{rot}$, the anisotropic contribution is modified, and a clear change in B_{hf} at each of the three Sn sites is observed (Fig. 5). In this state, the magnetization is essentially saturated so the hyperfine fields depend on the applied field, and the slope of B_{hf} vs B_o (for $B_o > 2.5$ T) is −0.94(8) for Sn 2c, −0.92(6) for Sn 2d, and −1.05(4) for Sn 2e, all consistent with the expected slope of −1 ($B_D \sim 0.5$ T in this geometry). The field dependence of B_{hf} for $B_o > B_{rot}$ was linearly extrapolated back to 0.5 T where the demagnetizating field should equal the applied field [see the saturation magnetization (Fig. 2)] to obtain $B_{hf}^{\mu \| c}$ for each tin site. B_{hf} measured in zero field yields $B_{hf}^{\mu \perp c}$ directly, and the difference δB_{hf}^A is the change in the anisotropic hyperfine field due to the 90° rotation of the moments. δB_{hf}^A is found to be large and negative for Sn 2e, and small and positive for Sn 2c and Sn 2d (Table II).

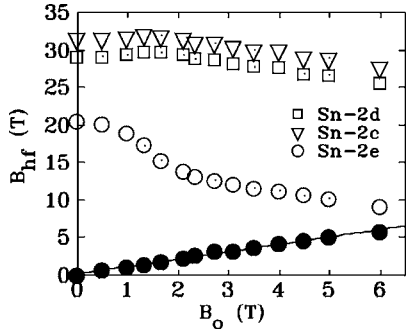

FIG. 5. Hyperfine fields at the three Sn sites in $YMn_6Sn_{5.42}In_{0.58}$ as functions of applied field. When the moments rotate onto the c axis, B_{hf} at the three Sn sites decreases. The solid line shows a linear fit to the field at the Sn impurity (filled circles) giving a slope of 0.97(3).

TABLE II. The change in anisotropic hyperfine field δB_{hf}^A, induced by a 90° moment rotation for the three Sn sites in $YMn_6Sn_{5.42}In_{0.58}$.

Site	δB_{hf}^A (T)
Sn 2c	1.9(8)
Sn 2d	2.1(3)
Sn 2e	−6.4(3)

IV. DISCUSSION

The total hyperfine field transferred to the Sn sites in $RMn_6Sn_{6-x}X_x$ has been assumed to be given by Eq. (1). This form ignores anisotropic contributions from magnetic rare-earth neighbors; a choice that may be justified as (i) the first neighbors of all three Sn sites are Mn atoms, with any rare-earth atoms being more distant,[15] and (ii) the hyperfine field at any given Sn site does not appear to be strongly affected by the presence or absence of a moment at the rare-earth site [compare data for the Y and Mg compounds in Table I with that for $ErMn_6Sn_{5.89}Ga_{0.11}$ (Ref. 9)]. We will return to this point later.

As the second term in the brackets in Eq. (1) is independent of moment direction, we need only consider the first term (denoted $\mathbf{A}_1$),

$$\mathbf{A}_1 = A_p \sum_{i=1}^{6} \mathbf{u}_i (\vec{\mu}_i \cdot \mathbf{u}_i). \tag{5}$$

In the $HfFe_6Ge_6$-type crystal structure, the Mn-Sn bonds make angles of 35° (Sn 2c and Sn 2d) and 73° (Sn 2e) with the c axis. In $YMn_6Sn_{5.42}In_{0.58}$, the Mn moments are in the ab plane for $B_o < B_{rot}$ and along c for $B_o > B_{rot}$ (from Mössbauer spectroscopy and magnetometry). At any given B_o, the angles and moment orientations are known, and $\mathbf{A}_1$ can thus be calculated for each Sn site (Table III, where $\Delta A_1/A_p$ is the change in $\mathbf{A}_1$ due to a rotation from the c axis to the ab plane). Since the signs of δB_{hf}^A (Table II) and $\Delta A_1/A_p$ (Table

TABLE III. Vector sum over the six Mn neighbors ($\mathbf{A}_1$) for the three Sn sites in RMn_6Sn_6 for Mn moments in the ab plane ($\vec{\mu} \perp c$) and along the c axis ($\vec{\mu} \| c$). Here, $\mu = \mu_{Mn}$.

Site	$\mathbf{A}_1/A_p$		$\Delta A_1/A_p$
	$\vec{\mu} \perp c$	$\vec{\mu} \| c$	
Sn 2c	$(0.72\mu, 0.72\mu, 0)$	$(0, 0, 3.96\mu)$	2.94μ
Sn 2d	$(0.69\mu, 0.69\mu, 0)$	$(0, 0, 4.04\mu)$	3.07μ
Sn 2e	$(1.95\mu, 1.95\mu, 0)$	$(0, 0, 0.48\mu)$	-2.29μ

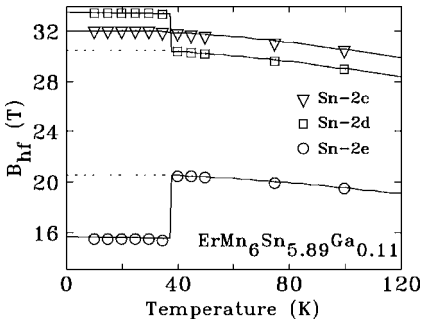

FIG. 6. Hyperfine fields at the three Sn sites as functions of temperature in $ErMn_6Sn_{5.89}Ga_{0.11}$ (Ref. 9). The spin reorientation occurs at T_{sr}=38(2) K, where the moments rotate from the c axis ($T<T_{sr}$) to the ab plane ($T>T_{sr}$). Note that the hyperfine fields for Sn 2c and Sn 2d exchange sequence at T_{sr} [emphasizing the importance of basing the site assignment on efg rather than B_{hf} (Ref. 9)]. The solid lines show Brillouin fits to the $T>T_{sr}(\mu\perp c)$ hyperfine fields and are continued as dotted lines below T_{sr}.

III) agree in all cases, the anisotropic and isotropic contributions to B_{hf} have the same sign in $YMn_6Sn_{5.42}In_{0.58}$.

From neutron scattering at 2 K, the Mn moment in $YMn_6Sn_{5.42}In_{0.58}$ (μ in Table III) was measured to be $\mu_{Mn}=2.57(9)\mu_B$. Therefore, $\mathbf{A}_1$ is known explicitly, and from it we can determine A_p, the anisotropic constant, through

$$A_p=\frac{\delta B_{hf}^A}{\Delta A_1}, \tag{6}$$

where δB_{hf}^A is the change in the anisotropic hyperfine field due to a rotation from the c axis to the ab plane (Table II) and depends only on the orientation of the Mn moments and their connecting bonds. A_p can be determined in other $RMn_6Sn_{6-x}X_x$ compounds provided μ_{Mn} and δB_{hf}^A are known. For the spin flop in $TbMn_6Sn_{5.46}In_{0.54}$, which occurs at 300 K in an applied field of B_{sf}=0.57(3) T,[6] $\mu_{Mn}=1.99(6)\mu_B$ [from $TbMn_6Sn_6$ at 300 K (Ref. 16)] and δB_{hf}^A is determined from an extrapolation to 0 T (the field was applied in the plane, so the demagnetization factor is zero). For the temperature-driven spin reorientations in $RMn_6Sn_{6-x}Ga_x$ (R=Tb,Er), we first determine the gap in B_{hf} at T_{sr}, then extrapolate this difference back to 0 K (on a Brillouin curve) to get δB_{hf}^A (Fig. 6 shows the hyperfine fields in $ErMn_6Sn_{5.89}Ga_{0.11}$ as an example[9]). Table IV summarizes the δB_{hf}^A and μ_{Mn} values for the compounds under investigation.

Using Eq. (1) and our data for the total and anisotropic hyperfine field contributions, we can determine the size of the isotropic constant A_s as well as the ratio A_p/A_s for each of the compounds studied here. Table V clearly shows that while the 2c and 2d sites exhibit essentially zero or modest effects, respectively, B_{hf} at the 2e site includes a substantial anisotropic contribution, with A_p being of the order of half of A_s in most of the materials shown in the table. The large values for A_p at the 2e site in these RMn_6Sn_6 compounds ($\sim 1T/\mu_B$) should be compared with the still larger values deduced from the study of $MnSn_2$ ($A_p=2.2T/\mu_B$).[2] It is worth noting that the local environments of the tin atoms in $MnSn_2$ and the 2e site in RMn_6Sn_6 compounds are very similar, characterized by comparable bond angles and lengths, although the atomic coordinations are different (4Mn+3Sn in $MnSn_2$ vs 6Mn+1Sn in RMn_6Sn_6). The anisotropic contribution to B_{hf} in $MnSn_2$ (and $FeSn_2$) was attributed to covalent bonding between the Sn and Mn (or Fe) atoms involving p-symmetry electrons. Since the local environment of the 2e site is comparable, it is likely that a similar mechanism could be invoked here. There are no other observations of anisotropic contributions to the hyperfine field for tin atoms in the prismatic coordination found at the 2c and 2d sites, so direct comparisons are not possible. However, the very much smaller values for A_p at these two sites suggest that the corresponding Mn-Sn bonds are either less covalent or involve less p character.

The results in Table V also highlight two other effects: (i) there is a trend associated with Ga doping levels in the ter-

TABLE IV. Change in anisotropic field δB_{hf}^A due to a rotation from the c axis to the ab plane and Mn moment values in $RMn_6Sn_{6-x}X_x$ (R=Tb,Er; X=Ga,In). μ_{Mn} is from neutron-scattering data on ternary RMn_6Sn_6 (R=Er,Tb) compounds. For the Ga-doped Er and Tb compounds, μ_{Mn} is taken at 2 K (δB_{hf}^A was calculated at 0 K), while for the In-doped Tb compound, the 300 K value was used (the spin flop occurs at room temperature). For the In-doped Y compound, we use μ_{Mn} measured at 2 K in $YMn_6Sn_{5.28}In_{0.72}$, which has the same ferromagnetic structure as $YMn_6Sn_{5.42}In_{0.58}$.

			δB_{hf}^A (T)			
R	X	x	Sn 2c	Sn 2d	Sn 2e	μ_{Mn} (μ_B)
Er	Ga	0.11	0.20(4)	3.1(1)	−5.1(1)	2.21(5)[a]
Tb	Ga	0.2	0.1(2)	3.3(1)	−5.5(1)	2.39(8)[b]
Tb	Ga	0.4	0.4(1)	3.7(1)	−5.3(1)	2.39(8)[b]
Tb	Ga	0.6	0.6(2)	3.9(2)	−4.9(1)	2.39(8)[b]
Tb	Ga	0.8	0.7(4)	4.1(3)	−5.0(3)	2.39(8)[b]
Tb	In	0.54	0.02(2)	2.38(4)	−4.1(1)	1.99(6)[b]
Y	In	0.58	1.9(8)	2.1(3)	−6.4(3)	2.57(9)[c]

[a]Reference 17.
[b]Reference 16.
[c]Reference 7.

TABLE V. Ratio of anisotropic to isotropic constants (A_p/A_s) in the $RMn_6Sn_{6-x}X_x$ compounds studied here (R=Y,Er,Tb; X=In,Ga).

	A_p/A_s (%)		
Compound	Sn 2c	Sn 2d	Sn 2e
$ErMn_6Sn_{5.89}Ga_{0.11}$	0.3(1)	5(1)	21(1)
$TbMn_6Sn_{5.8}Ga_{0.2}$	0.1(1)	4.8(1)	51(6)
$TbMn_6Sn_{5.6}Ga_{0.4}$	0.7(2)	5.6(4)	54(7)
$TbMn_6Sn_{5.4}Ga_{0.6}$	1.0(4)	5.9(6)	42(1)
$TbMn_6Sn_{5.2}Ga_{0.8}$	1.2(7)	6.3(7)	43(8)
$TbMn_6Sn_{5.46}In_{0.54}$	0	5.1(3)	72(10)
$YMn_6Sn_{5.42}In_{0.58}$	3(1)	4(1)	33(4)

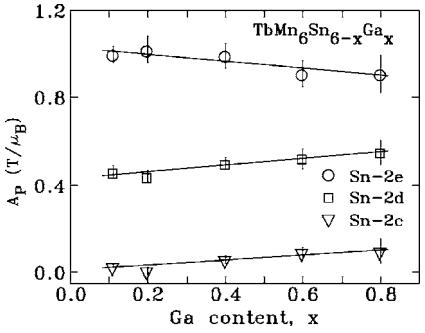

FIG. 7. Anisotropic constant for the three Sn sites in $TbMn_6Sn_{6-x}Ga_x$ ($0.2 \leqslant x \leqslant 0.8$). Solid lines are linear fits as guides to the eye.

bium compounds and (ii) replacing terbium by yttrium causes clear changes in the A_p/A_s ratio at the 2*c* and 2*e* sites. Figure 7 shows the composition dependence of A_p obtained through the temperature-induced spin reorientations in $TbMn_6Sn_{6-x}Ga_x$. The anisotropic constants for Sn 2*c* and Sn 2*d* grow at similar rates with increasing *x*, suggesting that larger Ga concentrations lead to greater anisotropic fields. In contrast, the much larger A_p for the Sn 2*e* site *decreases* with *x*. These data along with the anisotropic constants in $RMn_6Sn_{6-x}In_x$ (R=Tb, Y; moment rotation is B_o induced) are listed in Table VI. While there is broad agreement in A_p values for the three Sn sites in the In- and Ga-doped $TbMn_6Sn_6$ compounds, A_p for the Sn 2*d* site is clearly lower for In doping. Given the demonstrated composition dependence of A_p (Fig. 7) and the preference for the 2*d* site exhibited by both Ga (Ref. 8) and In,[6,12] it is likely that the nature of the dopant plays some small role in determining the anisotropic contribution to the total hyperfine field.

The differences between the two In-doped compounds in Table VI ($TbMn_6Sn_{5.46}In_{0.54}$ and $YMn_6Sn_{5.42}In_{0.58}$) cannot be attributed to the effects of the dopant or its concentration, so these compounds provide evidence that there is a significant contribution to A_p from the rare-earth moments in addition to the assumed contribution from the Mn moments. The effect is most striking at the Sn 2*c* site, which has three rare-earth neighbors, where the deduced A_p goes from essentially zero in the Tb compound to over $0.2T/\mu_B$ in the Y compound. This latter value is comparable with that of the 2*d* site in the same yttrium compound. As we are now explicitly considering the rare-earth contribution to be nonzero, normalization to the Mn moment is no longer appropriate, and we must compare the values of δB^A_{hf} shown in Table IV. The anisotropic fields at the Sn 2*d* sites are consistent within error, as might be expected since this site has no rare-earth neighbors. By contrast, the magnitude of δB^A_{hf} at both the 2*c* and 2*e* sites is about 2 T greater in the yttrium compound than in the terbium compound, and *both* of these sites have at least one rare-earth neighbor. We note that at both affected sites, the addition of a magnetic rare earth (Tb) leads to a *reduction* in $|\delta B^A_{hf}|$ and this may be a consequence of the antiparallel arrangement of the Mn and Tb moments. It is clear that the description of the transferred hyperfine fields provided by Eq. (1) is far from complete.

TABLE VI. Anisotropic constants (A_p) in some of the studied $RMn_6Sn_{6-x}X_x$ compounds (R=Y, Er, Tb; X=In, Ga).

Compound			A_p (T/μ_B)			
R	*X*	*x*	Sn 2*c*	Sn 2*d*	Sn 2*e*	Driving force
Er	Ga	0.11	0.03(1)	0.46(3)	1.00(4)	
Tb	Ga	0.2	0.01(2)	0.44(3)	1.02(6)	
Tb	Ga	0.4	0.06(2)	0.50(3)	0.99(6)	*T*
Tb	Ga	0.6	0.09(3)	0.52(5)	0.91(6)	
Tb	Ga	0.8	0.10(6)	0.55(6)	0.91(9)	
Tb	In	0.54	0.003(2)	0.39(2)	0.91(5)	B_o
Y	In	0.58	0.25(11)	0.27(5)	1.09(9)	
R neighbors			3	0	1	

V. CONCLUSIONS

We have investigated the anisotropic transferred hyperfine fields in $RMn_6Sn_{6-x}X_x$ (X=Ga, In) compounds with both magnetic (R=Tb, Er) and nonmagnetic (R=Y) rare earths. In every case, the transferred hyperfine field at the Sn 2*e* site has the largest anisotropic contribution, accounting for over 40% of the total B_{hf} in $TbMn_6Sn_{5.46}In_{0.54}$. We also found that the anisotropic fields from the Mn and rare-earth sublattices are quite similar in magnitude and can cancel, resulting in an apparently small net anisotropic field at the 2*c* site. While we have been able to isolate the Mn contribution to δB^A_{hf} by working with an yttrium compound, it would be of interest to investigate the rare-earth component of δB^A_{hf} directly by using a nonmagnetic 3*d* transition metal such as Cu or Ni. However, it is likely that the absence of 3*d* exchange interactions will drive the transition temperatures down to inconvenient values. Finally, the prismatic coordination of the tin atoms in the 2*c* and 2*d* sites appears to lead to greatly reduced anisotropic contributions, and a wider survey of magnetic stannides where this coordination is present could improve understanding of chemical bonding in this class of compounds.

[1] T. Mazet, J. Tobola, G. Venturini, and B. Malaman, Phys. Rev. B **65**, 104406 (2002).

[2] G. Le Cäer, B. Malaman, G. Venturini, and I. B. Kim, Phys. Rev. B **26**, 5085 (1982).

[3] G. Venturini, B. Malaman, G. Le Cäer, and D. Fruchart, Phys. Rev. B **35**, 7038 (1987).

[4] J. P. Sanchez, P. Vulliet, M. M. Abd-Elmeguid, and D. Kaczorowski, Phys. Rev. B **62**, 3839 (2000).

[5] G. Venturini, B. Chafik El Idrissi, and B. Malaman, J. Magn. Magn. Mater. **94**, 35 (1991).
[6] Laura K. Perry, D. H. Ryan, and G. Venturini, Hyperfine Interact. **170**, 105 (2006).
[7] C. Lefèvre, A. Verniére, G. Venturini, and B. Malaman, J. Alloys Compd. **361**, 40 (2003).
[8] Laura K. Perry, D. H. Ryan, G. Venturini, and J. M. Cadogan, J. Appl. Phys. **99**, 08J302 (2006).
[9] Laura K. Perry, D. H. Ryan, and G. Venturini, J. Appl. Phys. **101**, 09K504 (2007).
[10] F. Canepa, M. Napoletano, C. Lefèvre, and G. Venturini, Physica B **334**, 68 (2003).
[11] C. Lefèvre, G. Venturini, and B. Malaman, J. Alloys Compd. **351**, 65 (2003).
[12] C. Lefèvre, G. Venturini, and B. Malaman, J. Alloys Compd. **354**, 47 (2003).
[13] A. Matsuo, K. Suga, K. Kindo, L. Zhang, E. Brück, K. H. J. Buschow, F. R. de Boer, C. Lefèvre, and G. Venturini, J. Alloys Compd. **408-412**, 110 (2006).
[14] G. Venturini *et al.* (unpublished).
[15] B. Chafik El Idrissi, G. Venturini, and B. Malaman, Mater. Res. Bull. **26**, 431 (1991).
[16] B. Chafik El Idrissi, G. Venturini, B. Malaman, and D. Fruchart, J. Less-Common Met. **175**, 143 (1991).
[17] B. Malaman, G. Venturini, R. Welter, J. P. Sanchez, P. Vulliet, and E. Ressouche, J. Magn. Magn. Mater. **202**, 519 (1999).